Quasi-crystal structure: cold water on the Penrose tiling scheme

1990 J. Phys.: Condens. Matter 2 2499

(http://iopscience.iop.org/0953-8984/2/11/001)

J. Phys.: Condens. Matter **2** (1990) 2499–2517. Printed in the UK

Quasi-crystal structure: cold water on the Penrose tiling scheme

Marc de Boissieu†‡§, Christian Janot† and Jean-Marie Dubois‡

† Institut Laue–Langevin, 156X, 38042 Grenoble Cédex, France

‡ Laboratoire de Sciences et Genie des Matériaux Métalliques, Ecole des Mines, Parc de Saurupt, 54042 Nancy Cédex, France

Received 2 October 1989

Abstract. Quasi-crystalline structures are related to periodic distributions of $A3_{perp}$ volumes in a higher-dimensional space. If these $A3_{perp}$ volumes are actually confined inside the complementary space, three-dimensional Penrose lattice can be generated by the six-dimensional cut method. Diffraction data show that the actual $A3_{perp}$ must have components in the physical space, which make the three-dimensional structure description in terms of Penrose tiling not really reliable. Such 'parallel' components have been experimentally observed for the first time.

1. Introduction

Long-range ordered structure results not necessarily from periodic space tiling [1] and the notion of quasi-crystal, or quasi-periodic crystal, has been introduced to describe substances [2] that have a sharply peaked diffraction pattern and yet without any evidence for periodicity.

For periodic crystals, the structure is completely specified when both the unit cell (or the Bravais lattice) and the positions of atoms in this unit cell have been determined. The so-called direct methods of crystallography are the usual way to extract this structural information from diffraction data.

Basically, quasi-crystals must be treated the same way; position (indexing) of the diffraction peaks are related to the geometrical characteristics of the quasi-periodic framework while distribution of the scattered intensity should reveal where the atoms are located. The first step, i.e. the successful description of the quasi-periodic lattice, has been achieved with use of a variety of different schemes for generating them [1]: space tiling by two rhombohedral cells with matching rules, inflation–deflation procedure, multi-grid or dual methods, strip-projection [3] or cut-projection approaches [4]. The latter, in particular, drives quasi-crystals back to crystallography by showing that any three-dimensional quasi-periodic lattice has actually hidden translation invariances which can be recovered if the structure is properly described in a higher-dimensional

§ Present address: Laboratoire de Thermodynamique et Physico-chemie Métallurgiques, Ecole Nationale Supérieure d'Electrochemie et d'Electrométallurgie de Grenoble, BP 75, 38402 St Martin d'Hères Cédex, France.

0953-8984/90/112499 + 19 $03.50

space. For instance, the archetypical icosahedral quasi-crystals with $m\bar{3}\bar{5}$ point group symmetries cannot be periodic in three dimensions but there are three possible six-dimensional icosahedral periodic arrangements, i.e. the primitive (P), face-centred (F) and body-centred (I) cubic Bravais lattices. Each of them corresponds to well defined indexing (positions and extinction rules) of the diffraction peaks [5]. The second step, i.e. saying where the atoms are, is intrinsically more difficult for a quasi-crystal than for a crystal. A perfect quasi-periodic structure, without any disorder, still has an infinite number of sites in three dimensions which are not exactly equivalent. There are also practical difficulties to be overcome, related to the fairly low level of information that can be extracted from diffraction patterns of quasi-crystals. The diffraction pattern of a quasi-crystal, due to non-periodic long-range order, is singularly continuous (very dense set of Bragg-like reflections). In a typical powder diffraction experiment about 30–60 independent reflections only are actually measured. Thus, quite a large part of information is smeared out into the background. One way to recover this information partly is to use the so-called direct space method (DSM) [6]. In the DSM, currently employed for deciphering structural problems in non-crystalline materials, pair distribution functions (PDFs) and, possibly, partial pair distribution functions (PPDFs) can be obtained. In this approach, diffraction patterns are measured over a large Q-range and a continuous Fourier transform (FT) of the whole (normalised) scattering signal gives the averaged, isotropically regrouped probability of atomic pairs as a function of pair distances. Contrast variation with neutron diffraction allows the PPDF to be determined from convenient data sets. The negative point of such a procedure is that angular information is obviously lost, but the whole (diffuse) signal between the strong peaks is reintroduced into the FT and thus contributes to the PDF and/or PPDF. The method has been shown to be fairly reliable for investigating short- and medium-range order not only in liquids or amorphous materials but also, more recently, in ordered structures [6, 7]. Thus, quasi-crystallography *and* the DSM must be used jointly if one is to expect the best from the diffraction approach to quasi-crystal structures. The many intricacies of the direct methods have been very often bypassed or at least complemented by modelling approaches [8–12] as extensively reviewed elsewhere [13, 14].

The purpose of this paper is to reanalyse and complement neutron diffraction data, measured with an $Al_{74}Si_5Mn_{21}$ quasi-crystal, and to demonstrate that, while the average structure can be described in terms of decorated three-dimensional Penrose lattices, important details of this structure depart significantly from this scheme. After a summary of what quasi-crystallography is and a brief report on the direct treatment of diffraction data, it will be shown how experimental constraints request a certain extent of modelling, implying generalised atomic volumes, in the six-dimensional related structure, which are not entirely contained in the complementary (or perpendicular) space.

2. The six-dimensional cut scheme

The best way to analyse the relation between diffraction data and the structure of a quasi-crystal is probably to work out the problem within the so-called cut method.

In the cut method, an icosahedral quasi-periodic arrangement of atoms in the three-dimensional physical space $R3_{par}$ corresponds to a periodic arrangement of three-dimensional hypersurfaces, or atomic shells $A3_{perp}$ in six-dimensional space R6. These atomic shells intersect the three-dimensional real-world hyperplane at the atom positions. For physically obvious reasons, the $A3_{perp}$ cannot intersect each other and they have to be

invariant under the operations of the point group symmetry (120 in the case of $m\bar{3}\bar{5}$); they do not have to be hyperplanes. For each type (or family) of atomic sites in three dimensions there is one $A3_{perp}$ shell whose relative volume is directly related to the corresponding relative atomic three-dimensional density. In an idealistic monatomic icosahedral quasi-crystal, with a single site at the origin of the six-dimensional structure, and triacontahedral $A3_{perp}$ entirely contained in the $R3_{perp}$ space complementary to $R3_{par}$ in R6, the three-dimensional atomic density is a distribution of Dirac functions at the vertex positions of a three-dimensional Penrose tiling (3DPT). The volume of $A3_{perp}$ is equal to $n_3 a^6$ in which a is the six-dimensional lattice parameter and n_3 the three-dimensional atomic density. Correspondence rules also exist between the reciprocal spaces R6*, $R3^*_{par}$ and $R3^*_{perp}$, respectively. These reciprocal spaces contain the FTs of the densities and it is easy to demonstrate that the FT $F(\boldsymbol{Q}_{par})$ in $R3^*_{par}$ is the projection onto this very reciprocal subspace of the FT $F(\boldsymbol{Q}_6)$ in R^*_6; $F(\boldsymbol{Q}_6)$ in turn is a distribution of δ functions modulated by $G(\boldsymbol{Q}_{perp})$, the FT of $A3_{perp}$ ($\boldsymbol{Q}_{par}$ and $\boldsymbol{Q}_{perp}$ are the projections of $\boldsymbol{Q}_6$ onto $R3^*_{par}$ and $R3^*_{perp}$, respectively). Such a correspondence scheme is illustrated in figure 1, using a two-dimensional → one-dimensional simplification. The high-dimensional periodic structure is here a two-dimensional simple square lattice and the physical (parallel) space has been chosen for cut generating a one-dimensional quasi-crystal as a so-called Fibonacci chain (two tiles, of long and short distances, L and S, respectively, in a sequence $LSLSLLSLLSLSL\ldots$ resulting from the building rules $L \rightarrow LS$ and $S \rightarrow L$; in the present example $L/S = \tau$, the golden mean). A Fibonacci chain is the exact one-dimensional equivalent of a 3DPT.

The points of interest for an experimental approach to the quasi-crystal structures may then be summarised as follows.

(i) There is a one-to-one correspondence between $\boldsymbol{Q}_6$ and $\boldsymbol{Q}_{par}$ which generates a six-integer indexing of the diffraction peaks measured at $\boldsymbol{Q}_{par}$ in $R3^*_{par}$ and allows us to determine the six-dimensional Bravais lattice from diffraction data.

(ii) Intensities $|F(\boldsymbol{Q}_{par})|^2$ measured at $\boldsymbol{Q}_{par}$ in diffraction data are also the intensities $|F(\boldsymbol{Q}_6)|^2$ that would correspond to a 'six-dimensional diffraction experiment'.

(iii) The diffraction pattern in $R3^*_{par}$ is a very dense set of peaks whose intensity is a decreasing function of $\boldsymbol{Q}_{perp}$ due to the shape factor effect of $A3_{perp}$ (see figure 1).

(iv) The direct FT of these measured $F(\boldsymbol{Q}_6)$, or at least of $|F(\boldsymbol{Q}_6)|^2$, gives the six-dimensional structure (site positions *and* $A3_{perp}$ function), or at least the corresponding six-dimensional Patterson functions.

(v) The three-dimensional cut of this six-dimensional structure by $R3_{par}$ results in physical atom positions.

3. Application to the interpretation of diffraction data with an Al–Si–Mn quasi-crystal

Al–Si–Mn alloys are not monatomic nor single-sited systems. The immediate unavoidable complication with respect to the simple scheme as described in section 2 is that the $F(\boldsymbol{Q}_{par})$ and $F(\boldsymbol{Q}_6)$ structure factors contain several contributions such as

$$F(\boldsymbol{Q}_6) = \delta(\boldsymbol{Q} - \boldsymbol{Q}_6^{lat}) \sum_{\alpha} b_\alpha G_\alpha(\boldsymbol{Q}_{perp}) \exp(i2\pi \boldsymbol{Q}_6 \cdot \boldsymbol{r}_\alpha)$$

α being indicative of the atomic sites at position $\boldsymbol{r}_\alpha$ in the six-dimensional space; b_α are the scattering lengths of atoms sited at $\boldsymbol{r}_\alpha$ and G_α the FT of the pertinent volume $A3_{perp}(\alpha)$

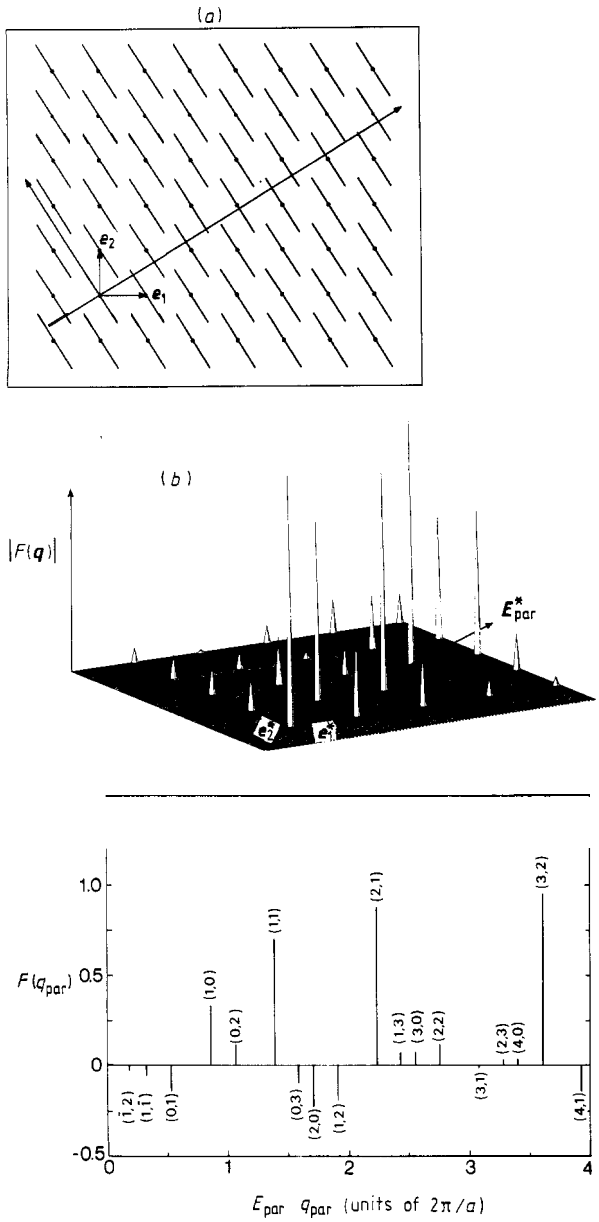

Figure 1. Illustration of the high-dimensional crystallography methods. Integrated intensities of the strong peaks are obtained from diffraction data. (*c*) They give at least amplitudes of the structure factors and two-integer indexing; (*b*) this two-integer indexing allows the high-dimensional diffraction pattern to be reconstructed; (*a*) Fourier transform of this pattern gives the high dimensional periodic structure which, when cut by our physical space, determines atom positions.

attached to each site. The FT of these $F(Q_6)$ gives correctly the lattice points in six dimensions but only *combinations* of the dephased $A3_{perp}(\alpha)$ atomic shells. This complication can be somewhat overcome by using contrast variation techniques in neutron

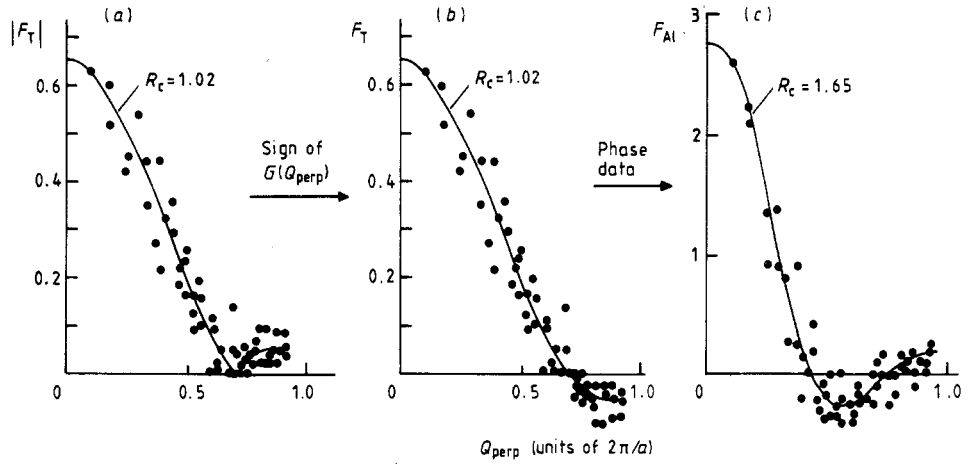

Figure 2. The amplitude of the partial structure factor $|F_T|$ for the transition-metal atoms depends on Q_{perp} as $|G(Q_{perp})|$ due to the one-site (origin) structure of the T sublattice in six dimensions. $G(Q_{perp})$ is an oscillating shape factor and goes from positive to negative values when passing through zero. Thus, (*a*) $|F_T(Q_{perp})|$ can be turned into (*b*) $F_T(Q_{perp})$ straightforwardly. The experimentally measured phase differences between F_T and F_{Al} (equal to zero or π) then gives (*c*) $F_{Al}(Q_{perp})$.

diffraction. Basically, isotopic or isomorphous substitutions allow us to vary the weight of one, or several, atomic species into the scattered signal. By measuring several diffraction patterns weighted differently, it is possible to calculate what would be the diffraction patterns if each atomic species were alone, i.e. the so-called *partial* structure factor. The problem can then be treated as the superposition of several monatomic structures.

As previously reported [15–18], it is possible to obtain icosahedral quasi-crystals $Al_{74}Si_5Mn_{21}$ and their modifications resulting from σ-FeCr substitution into Mn. Their neutron diffraction patterns can be indexed with six integers related to a six-dimensional icosahedral primitive lattice with a parameter $a = 6.5$ Å. The peak intensities can be written

$$I(\boldsymbol{Q}_{par}) = |b_{Al}F_{Al} + b_T F_T|^2$$

where the b-values are the neutron scattering lengths of Al + Si and transition-metal atoms, respectively; the F-values are the partial structure factors. In the experiment, b_{Al} is a constant while b_T can be varied from -0.373×10^{-12} to $+0.658 \times 10^{-12}$ cm. From at least three sets of diffraction data corresponding to samples with different b_T-values, $|F_{Al}|$, $|F_T|$ and $\cos(\widehat{F_{Al}, F_T})$ $(= \pm 1)$ in the present case) have been determined for every measured diffraction peak [15, 16].

The partial Patterson function in six dimensions calculated for the T atoms by direct FT of $|F_T|^2$ shows unambiguously that there is only one T site, at the origin of the six-dimensional cubic lattice. Thus the lattice contribution to the $\boldsymbol{Q}_6$-dependence of the F_T phases is a constant, as for any partial structure factor of periodic arrangements of lattice sites. The consequence is that F_T is related to $\boldsymbol{Q}_6$ through the Q_{perp}-dependence of $G_T(Q_{perp})$ only. This $G_T(Q_{perp})$ is the FT of a spatially finite volume $A3_{perp}(T)$ and, as such, is some sort of damped oscillating function. It is then possible to say that there are sign changes for $F_T(Q_{perp})$ at the Q_{perp}-values which correspond to the experimentally determined $|F_T(Q_{perp})|$ equal to zero [15, 16], as illustrated in figure 2. The phases of F_T,

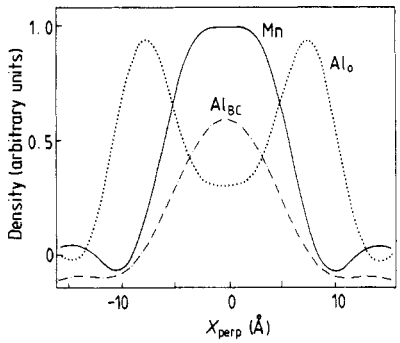

Figure 3. Density profiles of the T (origin), Al_o (origin) and Al_{BC} (body centre) $A3_{perp}$ volumes as deduced from neutron diffraction data. The profiles are scanned along a twofold axis in the complementary (perp) space.

equal to 0 or π, are thus reconstructed and the phases of F_{Al} follow from the measured values of $\cos(\widehat{F_{Al}, F_T}) = \pm 1$, as also illustrated in figure 2.

Now, the direct FT of F_T and F_{Al} in six dimensions gives the partial distribution of atomic sites convoluted by the pertinent atomic shells $A3_{perp}(T)$ and $A3_{perp}(Al)$, respectively. This six-dimensional structure is quite simple [15, 16]. As already seen in the partial Patterson function, there is only one site associated with the T atoms, at the origin of the six-dimensional cube, and two sites associated with the Al atoms, one also at the origin of the six-dimensional cube and the other at the body centre positions. The $A3_{perp}$ volumes have roughly spherical symmetries in $R3_{perp}$. Their density profiles, shown in figure 3, give their sizes and shapes; they do not have sharp borders that would correspond to constant density inside and zero outside but exhibit rather smeared limits. The $A3_{perp}(Al_o)$ has even an almost empty core which makes it shell shaped (figure 4). The six-dimensional structure may be visualised with a two-dimensional map of the sort shown also in figure 4. Thus the six-dimensional structure as deduced from neutron diffraction data can be considered as perfectly specified. The next step, in principle, is to generate atom positions in three dimensions by a pertinent physical cut of this six-dimensional structure. There is actually no basic difficulty in getting a list of atom coordinates [15, 16] but we are left with the problem of how to describe properly the three-dimensional structure. As the $A3_{perp}(T)$ volume attached to the transition-metal sites is not too different from the triacontahedron that would generate the vertices of a 3DPT, the simplest idea was an attempt to specify this three-dimensional structure with respect to an underlying 3DPT [15, 16]. Transition-metal sites have then been located at the vertices, and Al sites on the long diagonals of the rhombohedron faces (both prolate and oblate) and along the triad axis of the prolate rhombohedra (see [15, 16] for details) but, owing to the actual shape and/or low-density parts of the experimental $A3_{perp}$ volumes, the six-dimensional structure cannot induce a single perfectly defined decoration of the 3DPT rhombohedra. The resulting three-dimensional arrangement is only an *average structure* which, indeed, can be used as such for physical studies. The atomic sites as reported here are more than often partially occupied only. It is noteworthy that there is no mid-edge Al sites, contrary to what was formerly suggested in models based on Mackay icosahedron (MI) clusters [19] since the inner small Al icosahedron is not found and replaced by a half-occupied pentagonal dodecahedron. Fragments of filled Al–Mn small icosahedra are also found and the outer shells (large Mn icosahedron and large Al icosadodecahedron) of the MI are still observed. Unphysical short atomic pair distances are also generated, which suggests that spurious details of the experimental $A3_{perp}$ volumes have to be corrected for.

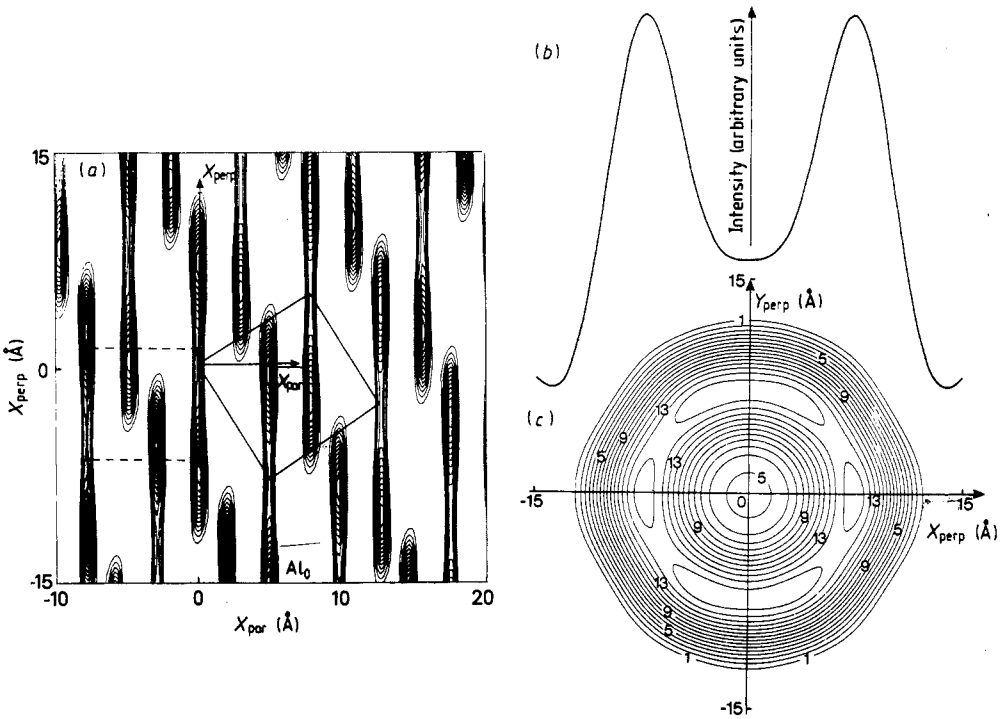

Figure 4. (*a*) Two-dimensional map of the six-dimensional density as obtained from the FT of the experimentally obtained partial structure factor. The map contains one twofold axis in $R3_{par}$ and another twofold axis in $R3_{perp}$; the density features are restricted to those corresponding to $A3_{perp}(Al_o)$. (*b*) Density profile. (*c*) Equal-density contours for the same $A3_{perp}(Al_o)$.

Further refinements are indeed possible, but several points must be advocated carefully if more elaborate conclusions have to be proposed confidently.

4. From experimental limitation to necessary modelling

In classical crystallography, the usual procedure to derive a structure is first to infer a 'raw' specification of atomic sites from diffraction data (both positions and intensity of the Bragg peaks) and then to refine atom positions; the 'raw structure' is back Fourier transformed into reciprocal space and the atom coordinates are adjusted for this FT to reproduce the diffraction data in the best way. Such a procedure offers the advantages of bypassing parasitic effects such as truncation in $\boldsymbol{Q}$-space, background problems, phase undetermination and Bragg peak degeneracies. The number of fitted parameters is of course reduced to the three coordinates per atom in the unit cell plus possible Debye–Waller factors to account for temperature and/or disorder effects. Transposition of the method to quasi-crystallography is easy in principle but actually far from being achievable. Direct refinement of the quasi-periodic three-dimensional structure, as described in section 3, is not possible because refining an 'average structure' is just nonsense. Moreover, Fourier transformation of an infinite complicated quasi-periodic

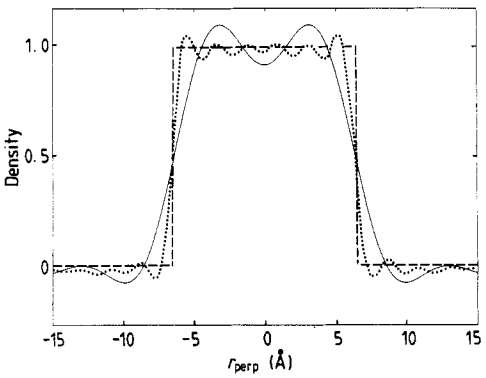

Figure 5. Illustration of the Q_{perp} truncation effects. The density profile in $R3_{perp}$ of a spherical $A3_{perp}$ function (– – –) is compared with profiles calculated by FTs of the $G(Q_{perp})$-function when cut at $Q_{perp} = 1$ (——) and $Q_{perp} = 3$ (· · · · ·). Ripples, depressions and border smearing are observed.

structure is not that straightforward. Refinement of the periodic six-dimensional description would indeed involve only the finite number of $A3_{perp}$ volumes contained in the six-dimensional unit cell and the corresponding attempt would look like classical crystallography, but for trivial dimensionality differences. Unfortunately, it is not that simple. The three-dimensional physical structure depends on size *and* shape of the $A3_{perp}$ volumes. If sizes can be fairly well obtained from diffraction data, shape details would need much more than the available information to be characterised properly. For instance, the $A3_{perp}$ experimentally obtained as explained in section 3 exhibit smeared spherical profiles, but it is not possible to state that this smearing is a true intrinsic feature because it may also come from truncation in Q_{perp}-space as explained elsewhere [15, 16, 20] and schematically summarised in figure 5. Thus, it would be unphysical to try a refinement procedure with many adjustable parameters that would hopefully describe the $A3_{perp}$ volumes! Moreover, even their overall spherical symmetry and their distribution on origin and body-centred sites must be actually questioned, as possibly resulting from measurement of the diffraction data on powder sample and not on single grain. Different Q_{par}-vectors (or Q_6-vectors) attached to non-equivalent Bragg reflections (with different intensities therefore) may contribute to powder diffraction peaks having the same modulus-Q-value. Without further assumption or experimental evidence, the total intensity of such a global peak can only be artificially shared uniformly between the contributing non-equivalent reflections, thus forcing isotropy of the structure. Fortunately, the reality does not seem to be that bad, as suggested by considering the experimental Q_{perp}-dependences of F_T and F_{Al} (figure 2) after limitation of the analysis to non-degenerated (simple) peaks. This is shown in figure 6. Obviously, the smooth regular behaviour still shows up and in particular $F_T(Q_{perp})$ is still very similar to the FT of a sphere. Then, positions, sizes and rough shapes of the $A3_{perp}$ volumes may be considered as globally correctly determined. They can be slightly modified by only small (or very small) additions or holes that must have no influence on the simple diffraction peaks. To quantify the point, let us consider a sort of counter-example in which the six-dimensional cube ($a = 6.5$ Å) would have an empty shell ($R = 6.2$–10.3 Å) at the origin and six filled spheres ($R = 5.2$ Å) on mid-edge positions. As shown in figure 7 the corresponding $F(Q_{perp})$ behaviour cannot be described by a smooth regular curve any longer. By trial and errors of this sort, it can be concluded that any $A3_{perp}$ reshaping or further modelling will *keep at least* 85% of the experimentally determined structure as described in the previous section and in [15, 16]. Finally, it must be also mentioned that the experimentally determined density in the six-dimensional structure is somewhat

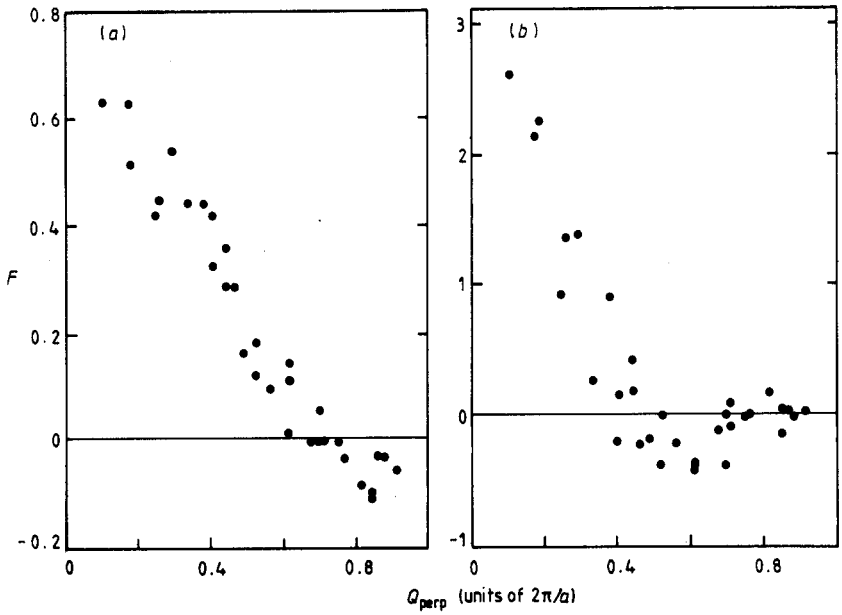

Figure 6. Q_{perp}-dependence of (*a*) F_T and (*b*) F_{Al} when the data are restricted to non-degenerated diffraction peaks.

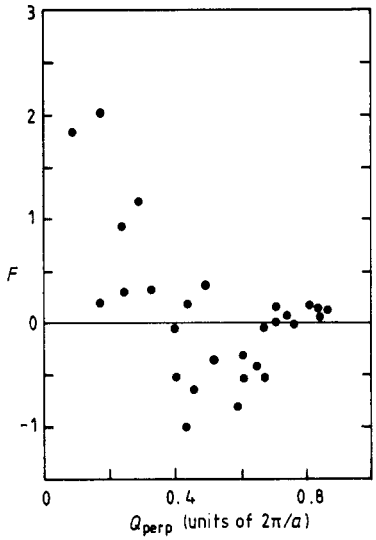

Figure 7. Simulation of a structure factor corresponding to an empty spherical shell at the origin of the six-dimensional cube plus six smaller spheres at mid-edge sites.

noisy (figure 8) and a background cut-off has to be defined before cutting the structure by the three-dimensional physical space; the choice of this cut-off level is not as irrelevant as it should be concerning the final three-dimensional physical structure.

Thus, if a complete physical structure of the quasi-crystal is to be specified, *modelling is not totally unavoidable* [11, 15]. The simplest thing to do is to keep spherical $A3_{perp}$ volumes. This has the minor and undercontrolled disadvantage of generating unphysical

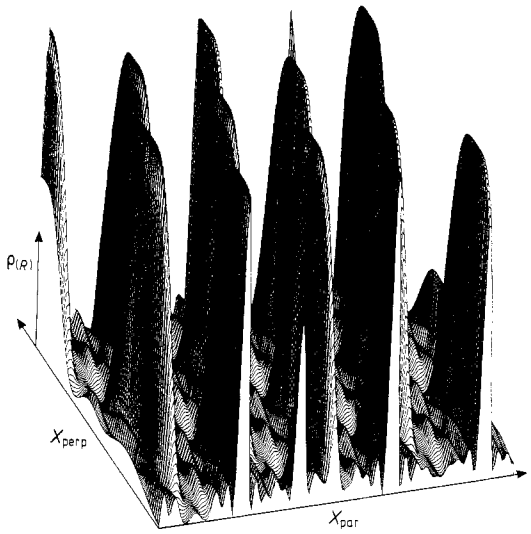

Figure 8. A perspective view of a two-dimensional density map of the six-dimensional partial substructure corresponding to the (origin) manganese $A3_{perp}$ volumes. The density is scanned in a plan containing one twofold axis in the physical space and one twofold axis in the complementary space. A significant background shows up in between the strong density features.

short pair distances in three dimensions as already stated. On the other hand the FT is, to the first order, more sensitive to volume than to shape. For instance, a sphere and a triacontahedron, with the same volumes, have almost indistinguishable FTs and, of course, the FT of a sphere is far more easily achieved! Initially, in the absence of evidence otherwise, these spheres are going to have sharp borders (constant density inside, and zero outside) and volumes equal to those of the experimental $A3_{perp}$. Thus the six-dimensional cube is going to be decorated as follows:

(i) $A3_{perp}(T)$: sphere at the origin with a radius of 6.18 Å and a full occupancy (constant density inside the sphere normalised to unity);

(ii) $A3_{perp}(Al_o)$: also at the origin but is an empty spherical shell surrounding $A3_{perp}(T)$ exactly; the radii are 6.18 and 10.3 Å and the occupancy is also equal to unity;

(iii) $A3_{perp}(Al_{BC})$: at the body centre with radius of 5.6 Å and 0.58 occupancy.

The corresponding structure in three-dimensions has a density of 3.62 g cm^{-3} and a composition $Al(o)_{71.4}Al(BC)_{8.9}T_{19.7}$ in consistency with the alloy's actual characteristics.

The next step is to calculate integrated intensities of the diffraction peaks predicted by this six-dimensional structure and to compare with the observed values of the whole set of neutron diffraction patterns. A refinement procedure is used with the following seven parameters: a scaling factor and two Debye–Waller factors DW_{par} and DW_{perp} for each of the three atomic sites. The DW_{par} are classical Debye–Waller factors, associated with (thermal, chemical and topological) disorder in the physical three-dimensional space, and related here to possible displacements or deformation of the $A3_{perp}$ volumes, with components completely contained inside $R3_{par}$ (physical space). The DW_{perp}, contrarily, are due to possible displacements of the $A3_{perp}$ into the complementary $R3_{perp}$ three-dimensional space [21]. This is the so-called phason disorder [22] which has been

observed in high-resolution electron microscopy images [23] and gives some understanding for the experimental broadening of the diffraction peaks. Such a phason disorder may correspond to 'vacancies', 'extra atoms' or collective tile flippings in the three-dimensional space, with respect to the idealistic structure. Recovering the 'relaxed' perfect structure would request long-distance diffusive processes. As this is unrealistic, phason disorders are considered as 'frozen'. Within isotropy assumptions, these DW_{perp} can be written as $\exp(-B_{perp}Q^2_{perp})$, in analogy to the usual phonon term [21]. This is equivalent to saying that the initial idealistic spherical $A3_{perp}$ must be convoluted with a Gaussian profile in the direct perp space [22].

The DW_{par} are found to be very large for the two Al sites and correspond to mean square displacements of the order of 0.1 Å which certainly includes a contribution from static disorders. The phason DW_{perp} is tremendously large for the Al_{BC} site and is the factor which influences mostly the fit quality. Its value corresponds to average displacements of $A3_{perp}(Al_{BC})$ in the complementary three-dimensional space equal to about 2.3 Å. These displacements are only of the order of 0.7 Å for the two $A3_{perp}(T)$ and $A3_{perp}(Al_o)$ sited at the origin of the six-dimensional cube. In all cases, this is perfectly compatible with the smeared nature of the $A3_{perp}$ sphere borders, as directly deduced from data [15, 16].

The weak point of such a model is its relatively poor ability to reproduce the measured integrated intensities of the Bragg peaks [24, 25]. This is illustrated in figure 9 where calculated intensities are compared with the measured intensities for the two extreme values of the used neutron contrast [15, 16]. Mismatching of model to data is also quite visible when comparing the PPDF [26] as shown in figure 10. It should be noted that any attempted models using spherical or not spherical $A3_{perp}$ volumes, with a variety of the permitted slight modifications [11, 12], have so far reached a comparable degree of unsuccessfullness when compared with neutron diffraction data. Thus a fundamentally different ingredient seems to be necessary if improvements are to be expected. The definition of this new ingredient will be the purpose of the next section.

5. Generalised $A3_{perp}$ volumes: the parallel component

In the model and the average structure described in sections 3 and 4, the nearest-neighbour Al–Al distance has in fact two main components: one at 2.59 Å comes from two Al_o sites on a threefold axis, and the other at 2.99 Å also from two Al_o sites but on a twofold axis; a third minor component at 2.85 Å is an Al_o–Al_{BC} pair (figure 11(*a*)). The Al–Al distribution as obtained from the DSM is more compact and centred on 2.82 Å (figure 10). Thus the actual structure seems to depart from the ideal average structure, the Al–Al shortest distances being expanded along threefold axes and contracted along twofold axes. This expansion–contraction modification is of the order of 0.2 Å. A similar trend is also visible on the Al–Mn PPDF which shows a drastic increase in the threefold axis pairs (2.59 Å) to the disadvantage of the twofold axis pairs (2.99 Å) (figure 10). The Mn–Mn pairs are less accurately determined and huge truncation oscillations have unfortunate screening consequences. However, a perfect Mn Penrose sublattice would give fivefold pairs at 4.6 Å (edges of the rhombohedra) and twofold pairs at 4.85 Å (face short diagonals); the DSM experimental pair distances are rather 4.5 Å and 4.99 Å, respectively. It is easy to realise that contracting some pair distances and expanding others simultaneously cannot be obtained by simple reshaping of the $A3_{perp}$ volumes. If size and/or shape are modified in such a way that the $A3_{perp}$ keep being entirely contained in the three-dimensional (perp) space, complementary to the physical space, the existing

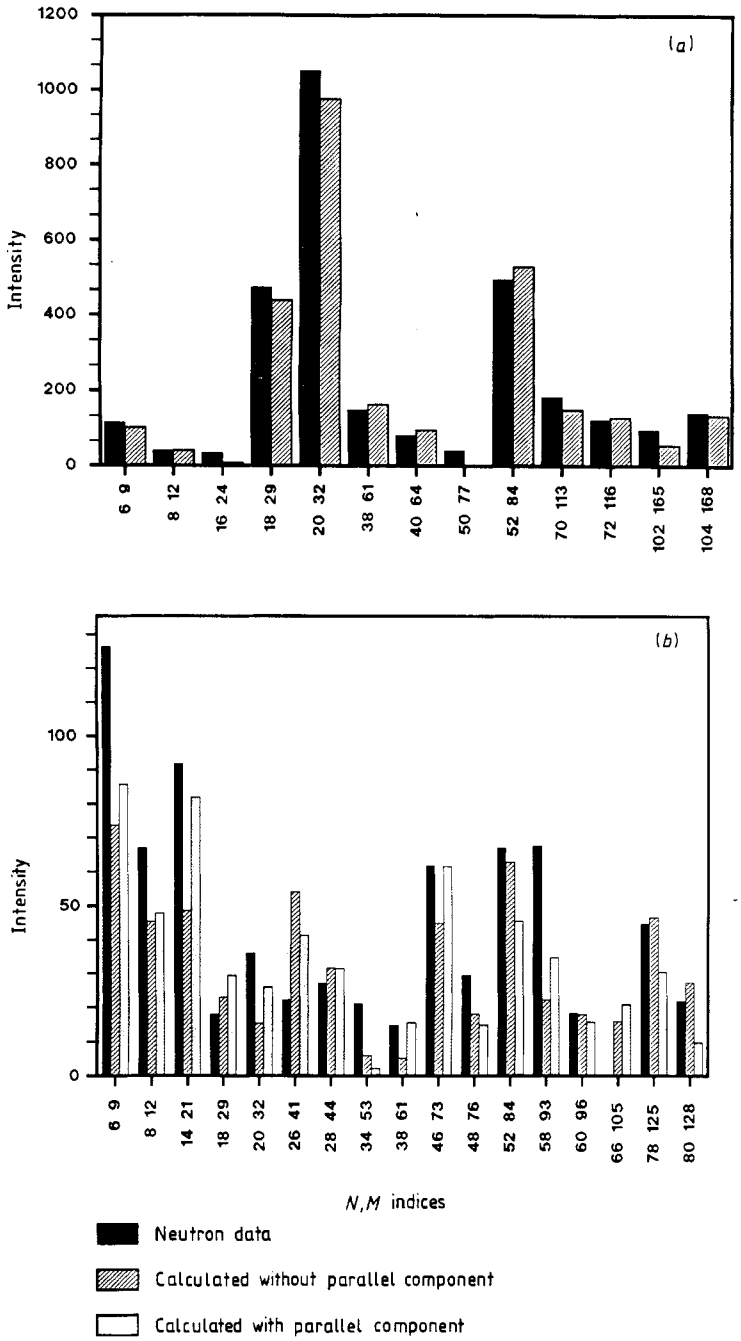

Figure 9. Calculated intensities compared with integrated intensities of neutron diffraction peaks measured in quasi-crystalline alloys: (*a*) $Al_{74}Si_5(FeCr)_{21}$ ($b_T = +0.658 \times 10^{-12}$ cm; similar to x-ray contrast with $Al_{74}Si_5Mn_{21}$); (*b*) $Al_{74}Si_5Mn_{21}$ ($b_T = -0.373 \times 10^{-12}$ cm). The calculated intensities have been obtained within the spherical approximation with or without parallel components as explained in the text. In (*a*) the measured and calculated intensities compare reasonably well and are not very sensitive to the parallel component. In (*b*) the agreement is poorer but improves when parallel components are introduced.

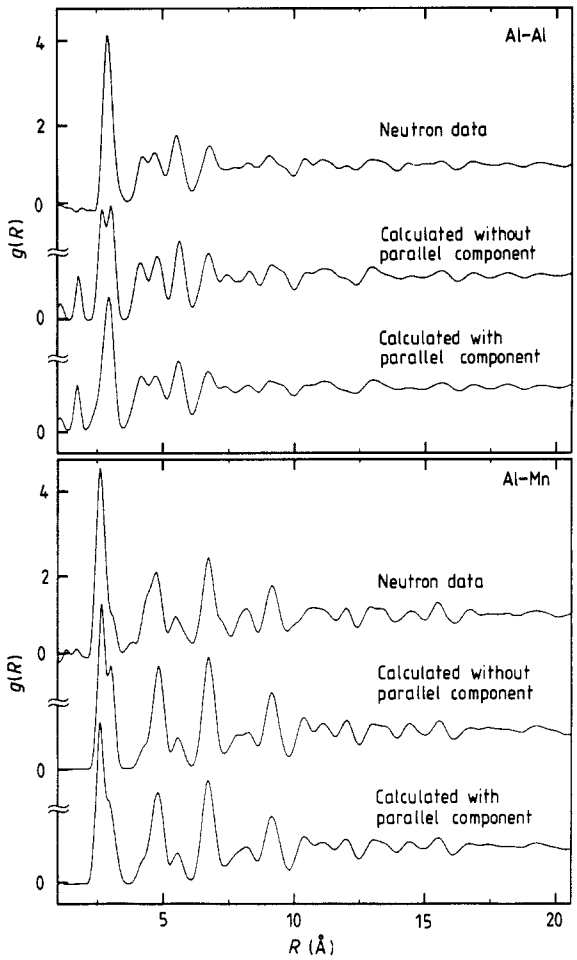

Figure 10. Partial pair distribution functions of the icosahedral $Al_{74}Si_5Mn_{21}$ phase directly measured by the DSM and calculated within the spherical approximation as explained in text. The agreement between data and simulation is obviously improved by the parallel component effect which reduces, in particular, the spurious splitting of the pair distances around 2.5–2.8 Å. The actual pair distributions, as shown in figure 11, have been given an artificial Gaussian broadening to simulate both resolution and Debye–Waller effects. The Mn–Mn correlations are poorly determined experimentally and they are not shown here for reasons explained in the text.

pair distances do not change except that some of them may disappear while new ones are created. The only way to produce expansion–contraction modifications in the structure is to give the '$A3_{perp}$' a certain amount of features, in the physical space, that will be called *parallel components* hereafter. Basically, such parallel components are not going to induce atomic disorder as long as the icosahedral symmetry is still respected. The diffraction peaks will remain sharp (Bragg like) and diffuse scattering will not be produced. One simple example, again using a two-dimensional–one-dimensional relation, is shown in figure 12, reproducing part figure 1(*a*). The initial A_{perp} are straight segments and a convenient cut of the two-dimensional structure by a physical one-dimensional space generates a Fibonacci sequence of two *L* and *S* distances. Shifting

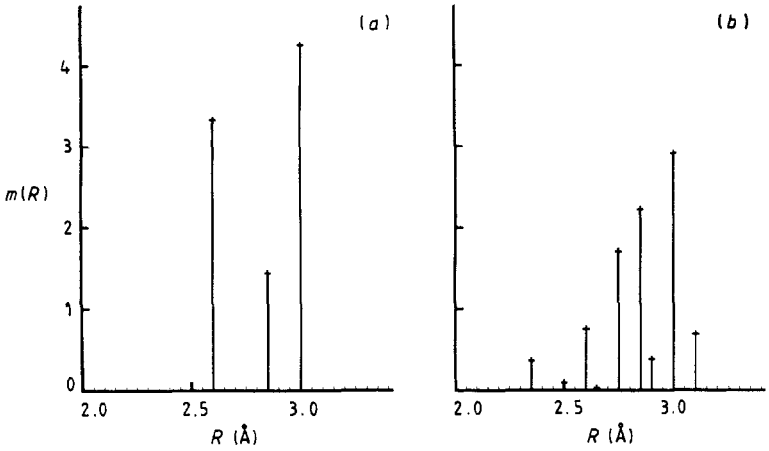

Figure 11. Actual pair distributions in the Al–Al correlations, without broadening, calculated as for simulations in figure 10. (*a*) The three components of the resolved 'doublet' around 2.8 Å transform into (*b*) a regular unresolved distribution of eight distances upon introduction of parallel components into the $A3_{perp}$ volumes.

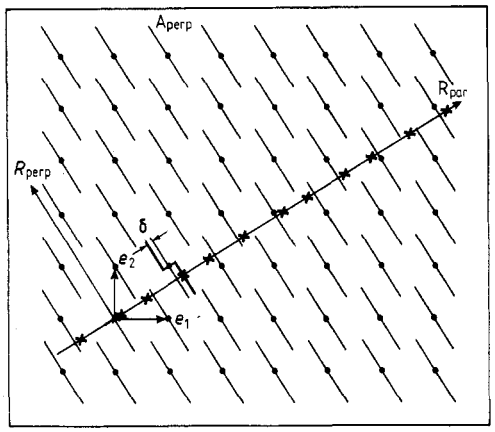

Figure 12. A simple illustration of how the one-dimensional Fibonacci sequence is affected by a parallel component δ of the A_{perp} segment. The short distances increase by 2δ, some long distances are reduced by 2δ and some other long distances are kept as such. The one-dimensional quasi-periodic structure is not a Fibonacci sequence any longer (×). Only one A_{perp} has been modified for clarity.

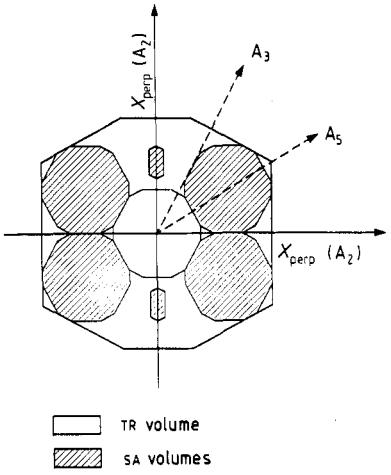

Figure 13. Schematic representation of the TR volume (triacontahedron) decorating the Mn sites in the six-dimensional structure. This is a two-dimensional cut of TR in complementary space, showing four of the 12 sA volumes that are going to be given a parallel component [12, 28].

antisymmetrically the two halves of the A_{perp} segments by a δ displacement entirely contained in the physical (par) space results in the expansion of the S distances up to $S' = S + 2\delta$ and the contraction of some L distances down to $L' = L - 2\delta$. The former

Fibonacci sequence $LSLSLLSLLSLSL\ldots$ becomes $L'S'L'S'LL'S'L'LS'L'S'\ldots$, which is another perfectly ordered sequence of *three* distances L, L' and S'. Many other modified structures can be generated if only small various parts of the A_{perp} segments are moved antisymmetrically.

To illustrate the point further in the periodic six-dimensional–quasi-periodic three-dimensional structure, an example will be given using ingredients taken from the model in [12]. In this model, the $A3_{perp}$ volumes attached to Mn and Al atomic sites are generated using three elements:

(i) a triacontahedron TR, whose centre-to-vertex distance along a fivefold axis is 7.44 Å (if $a = 6.5$ Å in six-dimensions); the three-dimensional physical cut of TR gives a 3DPT

(ii) a volume called A obtained by intersecting a τ-inflated TR with a regular dodecahedron of fivefold radius equal to 9.74 Å ($=a\tau^3/2\sqrt{2}$);

(iii) a volume sA which is a τ^3-deflated A volume and has a radius equal to 2.3 Å; sA is almost spherical.

As stated, the three-dimensional cut structure is a perfect 3DPT if TR is taken as an $A3_{perp}$ volume attached to the origin sites of a six-dimensional primitive cubic lattice. Vertices of the 3DPT are arranged in icosahedra. It has been demonstrated [12, 27] that the centres of these icosahedra result from the three-dimensional physical cuts of an sA volume at the central core of TR. Simultaneously, the 12 vertices of these icosahedra are generated by the physical cuts of 12 sA volumes which are translated from the central sA by vectors equivalent to $[a/\sqrt{2(2+\tau)}](\tau, 1, 0)_{perp}$. This situation is illustrated in figure 13. In the three-dimensional structure, centre-to-vertex distances are then defined by vectors equivalent to $(1, \tau, 0)_{par}$ and are equal to 4.62 Å (edges of the 3DPT). If the $A3_{perp}$ volume is modified (different shape, different volume, holes here and there, etc) in such way that it remains confined inside the complementary space, these distances will be kept unchanged; the only consequences may be the appearance of new (shorter) distances and the disappearance of a fraction of the pre-existing distances. Let us take now the 12 small sA volumes, as defined above, whose centres have coordinates in six-dimensional space given by vectors equivalent to $(\tau, 1, 0)_{perp} + (1, \tau, 0)_{par}$; without modifying the rest of TR, the 12 sA spots can be shifted, *into the physical space*, to position $(\tau, 1, 0)_{perp} + (1, \tau, 0)_{par} + \alpha(1, \tau, 0)_{par}$ [28]. The obvious effect of the extra parallel component $\alpha(1, \tau, 0)$ is to expand ($\alpha > 0$) or to contract ($\alpha < 0$) the icosahedron size, but the icosahedral symmetry is not altered and the three-dimensional generated structure is still quasi-periodic. In this example, the parallel component modifies about 60% of the initial structure, which means that 60% of the atomic sites are shifted with respect to the 3DPT vertices, to an extent depending on the magnitude of the chosen parallel component. How should it affect the diffraction data? The structure factor of the initial structure is proportional to $G_0(\boldsymbol{Q}_{perp})$, the FT of the TR volume. Shifting the 12 small sA volumes from $\boldsymbol{r}_6(k)$ to $\boldsymbol{r}_6(k) + \delta\boldsymbol{r}_{par}(k)$ modifies this structure factor by

$$\Delta = \sum_{k=1}^{12} G_k(\boldsymbol{Q}_{perp}) \exp[i\boldsymbol{Q}_6 \cdot \boldsymbol{r}_6(k)][1 - \exp(i\boldsymbol{Q}_{par} \cdot \delta\boldsymbol{r}_{par})]$$

in which $G_k(\boldsymbol{Q}_{perp})$ is the FT of a small volume sA. Because of size differences between sA and TR, the maximum value of $G_k(\boldsymbol{Q}_{perp})$ is about 30 times smaller than that of $G_0(\boldsymbol{Q}_{perp})$; G_k is also weakly variable in the Q_{perp}-range which shows that G_0 decreases to zero. The signs of Δ will depend on Q_6. Thus, introducing parallel components into

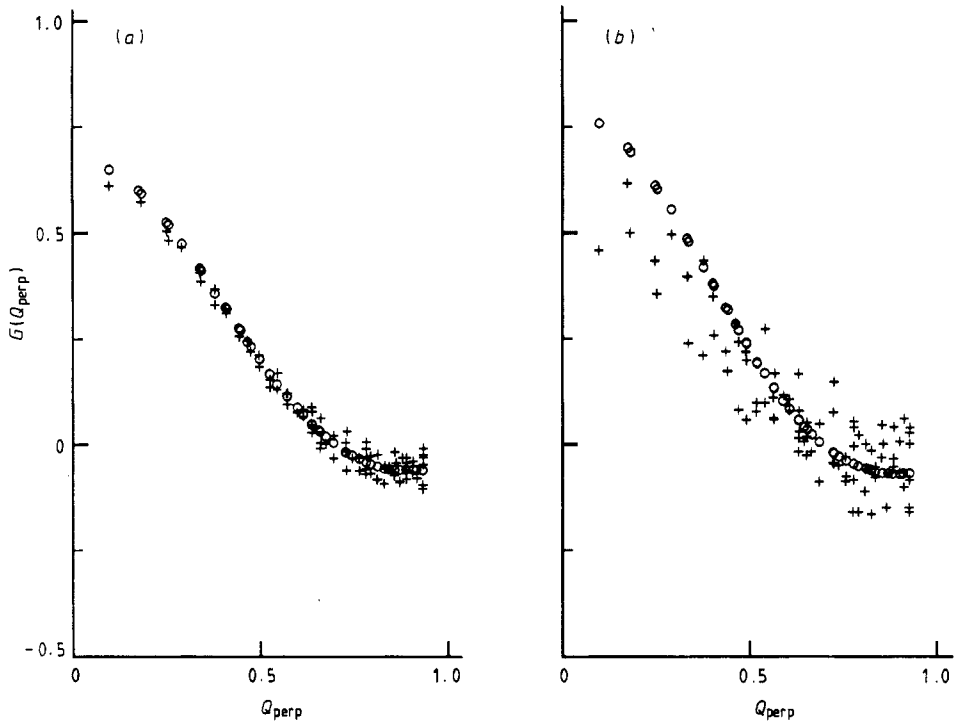

Figure 14. The $G(Q_{perp})$-functions, FTs of the $A3_{perp}$ volume, corresponding to a simple spherical profile (○) or showing effects due to parallel components (+) for 12 smaller spheres displaced along the physical fivefold axes by (*a*) 0.1 Å or (*b*) 0.5 Å.

the '$A3_{perp}$' volumes should have an effect mainly upon small-intensitydiffraction peaks (large Q_{perp}) and will also remove isotropy degeneracies. This conclusion is illustrated in figure 14, showing the $G(Q_{perp})$ function for two different parallel components, namely -0.1 and -0.5 Å. The largest value, certainly unrealistically too large, is visible on a pertinent two-dimensional map of the simulated six-dimensional structure (figure 15). Realistic parallel components might have more tiny effects on diffraction data, which are even less visible on the deduced six-dimensional structure owing to smearing truncation effects of the FT procedure and background cut-off. This is probably the strongest advocacy for a necessary touch of modelling to go beyond structural features directly obtained from data, even if a careful examination allows us, after all, to 'see' experimental parallel components (figure 15) which seems to follow the trend observed in the simulated structure.

In an attempt to test further the assumption of such parallel components, the simplistic model as described in section 4 has been modified accordingly. The $A3_{perp}(T)$ sphere related to the manganese sites at the origin has been given a parallel component for the 12 fivefold small spheres of volume sA as explained previously in this section. The $A3_{perp}(Al_o)$ empty spherical shell attached to the aluminium sites at the origin has been modified similarly by shifting 30 small spheres of volume sA along the twofold axes in the three-dimensional physical space. The parallel components have been considered as adjustable parameters in an attempt to fit the neutron diffraction data. Such a

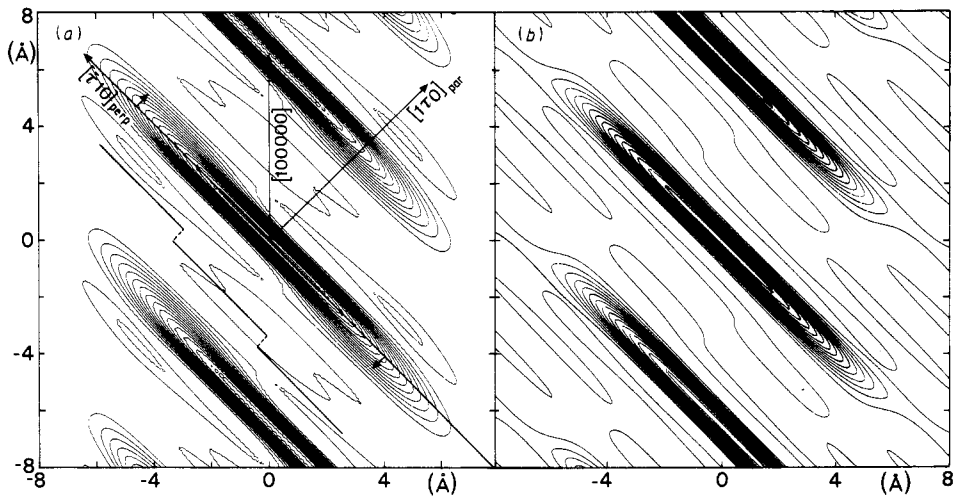

Figure 15. FTs of the partial structure factor F_{Mn}: (*a*) calculated with an $A3_{perp}$ volume based on a sphere with 12 smaller spheres shifted along parallel fivefold axes [28]; (*b*) deduced from diffraction data. The maps are two-dimensional cuts of the six-dimensional structures containing fivefold axes (one physical fivefold axis and one complementary fivefold axis). The simulated density map corresponds to the FT of a set of calculated F_{Mn}, within the spherical approximation as explained in the text and exactly equivalent to the measured set of values (same reflections); consequently, truncation effects are expected to spoil experimental and simulated densities to comparable extents.

procedure, as suggested in [28], is somewhat equivalent to the atomic position fitting of classical crystallography. The best fit, as pictured in figure 9, is obtained for $\delta r_{\|A5}(Mn) \simeq +0.14$ Å and $\delta r_{\|A2}(Al_o) \simeq -0.25$ Å which means that, with respect to the initial 3DPT, the Mn icosahedron radius has been expanded from 4.6 to 4.74 Å while the external Al icosadodecahedron radius has been contracted from 4.83 to 4.58 Å. Comparing the results shown in figure 9 illustrates an obvious improvement in reproducing diffracted intensities (the χ^2- and R-factors have been reduced by a factor of about 2) even if some of the diffraction peaks are still far from being correctly interpreted. An example is the peak corresponding to $N, M = 66, 105$ which should strongly constrain any model by its unexpected absence in the set of measured intensities. The calculated PPDFs are of course also sensitive to the presence of parallel components in the $A3_{perp}$ volume. The curves displayed in figure 10 show the good trends of the attempt. The Al–Al and Al–Mn partials are now quite nicely reproduced. (The Mn–Mn pairs, as reported, are more poorly determined and have not been used here to support any model although showing the same trend as the Al–Al and Al–Mn pairs.) Again spurious short distances show up, but there is no point in bothering too much about it as long as we know that they are due to the spherical approximation of the $A3_{perp}$ volumes. However, it is fair to point out that these spurious short distances may have a dramatic effect if the model is to be used for the prediction of physical properties. One can reasonably anticipate a final satisfactory description of the structure when non-spherical $A3_{perp}$ volumes, with pertinent parallel components as described in this section, are used. This approach, which is very simple in principle but quite tedious in practice, is in progress. It is already clear that the problem is of the multiple-parameter type. Physical constraints must be injected

into the determination of the '$A3_{perp}$' parallel components which, otherwise, are not unique.

The main effect of the parallel component is, as explained in this section, contraction–expansion of the successive icosahedral atomic shells, or fragments of them, with respect to those expected from a 3DPT. This is illustrated in figure 11 for the particular case of the Al–Al correlations. Thus, even if the 3DPT remains a good framework for the description of the average structure, the rhombohedral tiles are distorted enough to suggest a better picture of the actual structure in terms of statistical clusters, also derivable from a six-dimensional cut scheme. One might be also tempted to introduce the notion of 'modulated 3DPT'. It should be noted that these parallel parts of the $A3_{perp}$ volumes are reminiscent of the commensurate displacive modulations, as introduced in [14] in order to stabilise 3DPT structures. Such displacive modulations have actually been observed when simulating structure relaxation [14] or growth process [29, 30] for two-dimensional quasi-crystals. Chemical modulations related to phason disorder can also be generated in a similar way by substituting a small fraction of a given $A3_{perp}$ with the same volume taken from another $A3_{perp}$ (for instance Al $\Leftrightarrow$ Mn substitution). In [31, 32] it was also previously mentioned that detailed structures of quasi-crystals might be difficult to specify completely, owing to complicated shapes of the $A3_{perp}$ volumes including components in the physical space. It is fair to point out that somewhat successful attempts have been made to keep some kind of 3DPT description [8], but this is at the cost of using τ^3-inflated decorations with probably little benefit with respect to what would be a large unit-cell periodic structure approach. As explained also in this section, the parallel components do not induce any atomic disorder, as long as they are kept constant in six-dimensional space. The wavy background which shows up in the baseline of some of the diffraction patterns must have a different origin and is indeed the signature of true disorder. In that respect, space fluctuations of the parallel components might contribute to this disorder which, by the way, is taken into account, whatever the outcome, in the DSM approach.

6. Conclusion

The six-dimensional crystallography scheme is definitely a valuable tool for deriving the basic features of icosahedral quasi-crystals. For the simple systems and with the use of contrast variation effects, average structures are obtained which can be refined through a necessary last-step modelling for comparison with partial pair distribution functions and integrated diffracted intensities. Differences, with respect to this average structure, can be interpreted in terms of parallel components of the $A3_{perp}$ volume. This makes the description of the quasi-crystal structure on a 3DPT basis less realistic than suggested earlier. Qualitatively, the same kinds of icosahedral atomic shell are still present in the structure, including for instance fragments of the famous MIS [11], but they are rather strongly deformed. Connected statistical clusters are probably the best alternative way to specify quasi-crystal structure.

References

[1] Janot Ch and Dubois J M 1988 *J. Non-Cryst. Solids* **106** 193
[2] Shechtman D, Blech I, Gratias D and Cahn J W 1984 *Phys. Rev. Lett.* **53** 1951

[3] Duneau M and Katz A 1985 *Phys. Rev. Lett.* **54** 2688
[4] Bak P 1985 *Phys. Rev. Lett.* **54** 1517
[5] Cahn J W, Shechtman D and Gratias D 1986 *J. Mater. Res.* **1** 13
[6] de Boissieu M, Janot C, Dubois J M, Audier M and Dubost B 1989 *J. Physique* **50** 1689
[7] Egami T, Dmowski W, Jorgensen J D, Hinks D G, Capone D W, Segre C U and Zhang K 1987 *Rev. Solid State Sci.* **1** 247
[8] Audier M and Guyot P 1988 *Quasicrystalline Materials* ed C Janot and J M Dubois (Singapore: World Scientific) p 181
[9] Audier M and Guyot P 1988 *Phil. Mag. Lett.* **58** 17
[10] Guyot P, Audier M and de Boissieu M 1989 *Preprint 3rd Int. Meet. on Quasicrystals (Mexico) 29 May–2 June 1989, preprint*
[11] Cahn J W, Gratias D and Mozer B 1988 *J. Physique* **49** 1225
[12] Duneau M and Oguey C 1989 *J. Physique* **50** 135
[13] Janot C and Dubois J M 1988 *J. Phys. F: Met. Phys.* **18** 2303
[14] Janssen T 1988 *Phys. Rep.* **168** 55
[15] Janot C, Dubois J M, Pannetier J, de Boissieu M and Fruchart R 1988 *Quasicrystalline Materials* ed C Janot and J M Dubois (Singapore: World Scientific) p 107
[16] Janot C, de Boissieu M, Dubois J M and Pannetier J 1989 *J. Phys.: Condens. Matter* **1** 1029
[17] Janot C, Pannetier J, Dubois J M and de Boissieu M 1989 *Phys. Rev. Lett.* **62** 450
[18] Dubois J M and Janot C 1987 *J. Physique* **48** 1981
[19] Guyot P and Audier M 1985 *Phil. Mag.* B **52** L15
Audier M and Guyot P 1986 *Phil. Mag.* B **53** L43
[20] de Boissieu M, Janot C and Dubois J M 1988 *Europhys. Lett.* **7** 593
[21] Kalugin P A, Kitayev A Y and Levitov L S 1985 *J. Physique Lett.* **46** L601
[22] Levine D, Lubensky T C, Ostlund S, Ramaswamy S, Steinhardt P J and Toner J 1985 *Phys. Rev. Lett.* **54** 1520
[23] Wang D N, Ishimasa T, Nissen H U, Novmöller S and Rhyner J 1988 *Phil. Mag.* A **58** 737
[24] de Boissieu M 1989 *Thesis* University of Nancy; *Institut Laue–Langevin Internal Report*
[25] Janot C, de Boissieu M and Dubois J M 1989 *Anniversary Adriatico Research Conf. on Quasicrystals (Trieste) 4–7 July 1989* (Singapore: World Scientific)
[26] Dubois J M, de Boissieu M, Janot C, Dubost B, Fruchart R and Audier M 1988 *J. Non-Cryst. Solids* **106** 217
[27] Henley C L 1985 *J. Non-Cryst. Solids* **75** 91
[28] Duneau M 1989 private communication
[29] Nori F, Ronchetti M and Elser V 1988 *Phys. Rev. Lett.* **61** 2774
[30] Leung P W, Henley C V and Chester G V 1989 *Phys. Rev.* B **39** 446
[31] Bak P 1986 *Scr. Metall.* **20** 1199
[32] Bak P 1986 *Phys. Rev. Lett.* **56** 861